Electronic Supplementary Material (ESI) for Journal of Materials Chemistry A.

Supporting Information for

On the electrochemical origin of the enhanced charge acceptance of lead-carbon electrode

Wenli Zhang[a], Haibo Lin [a,b*], Haiyan Lu[a*], Dechen Liu[a], Jian Yin[a], Zheqi Lin[a]

a. College of Chemistry, Jilin University, Changchun 130012, China

b. Key Laboratory of Physics and Technology for Advanced Batteries of Ministry of Education, Jilin University, Changchun, 130012, China

* *Corresponding author. Tel.: +86 431 85155189; fax: +86 431 85155189 E-mail address:* lhb910@jlu.edu.cn (H. Lin),

luhy@jlu.edu.cn (H. Lu)

1. Experimental section

1.1 Fabrication of Pb and Pb/AC electrode

Electrolytic lead plate (working area of 1×1 cm^2, purity > 99.99%) was served as the Pb electrode. Firstly, the Pb electrode was polished with emery paper to a mirror surface. Then, it was rinsed orderly with acetone and deionized water. Finally, the non-working surfaces of Pb electrode were sealed with epoxy resin.

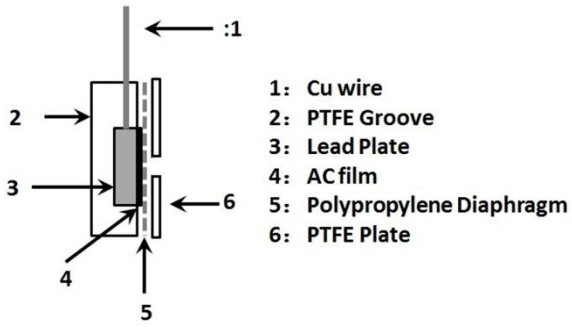

Fig. S1. Schematic diagram of the Pb/AC electrode.

Since it is difficult to separate the electrochemical contribution of activated carbon (AC) and lead in a pasted type lead-carbon electrode,[1] a Pb/AC electrode (Fig. S1) with excess AC was designed to simulate the electrochemical processes of AC in lead-carbon electrode, providing the presence of $Pb/PbSO_4$ redox couple. The Pb/AC electrode was assembled by pressing the AC film on a Pb electrode. A commercial AC (YP-50F, Kuraray, Japan) (properties shown in Table S1) was used as the active material of AC film, acetylene black was used as conductive additive and PTFE was used as binder in the AC film. The Kuraray AC is a commonly used AC in supercapacitors with moderate specific surface area, high purity and a relatively high bulk density. Hence we

choose this kind of AC for experiment.

Table S1 Properties of YP-50F AC

Density	Conductivity	Size	Ash	S_{BET}	V_{total}	V_{Micro}	V_{meso}
g cm^{-3}	S cm^{-1}	μm	%	m^2 g^{-1}	cm^3 g^{-1}	cm^3 g^{-1}	cm^3 g^{-1}
0.37	*ca.* 1.05[a]	5-8	0.3	1660	0.74	0.53	0.21

[a] the conductivity of AC powder varies with measurement method, particle size, pressure and so on.

The AC film was prepared by mixing AC (85 wt%), acetylene black (10 wt%) and PTFE (5 wt%) to form a mixture with ethanol soaking. Then, the mixture was rolled into a film (4 mg, 1 × 1 cm^2) with ethanol soaking. Subsequently, the AC film was dried in a vacuum drying oven at 100 °C overnight to evaporate ethanol. Finally, the AC film was pressed onto the surface of Pb electrode to fabricate the Pb/AC electrode. In order to avoid the shedding of AC film from lead surface, a PTFE plate with a hole (diameter ϕ = 1 mm) was pressed on the surface of AC film. The AC film, lead and PTFE plate was bound together to fabricate the Pb/AC electrode. The hole in PTFE plate was designed to measure the potential of Pb/AC electrode with the assistance of a Luggin capillary. Deionized water and analytical grade reagent were used in all experiments.

1.2 Electrochemical and physical characterizations

Alternating current electrochemical impedance spectroscopy (EIS), Chronoamperometry, cyclic voltammetry, and other electrochemical characterization of Pb and Pb/AC electrodes were carried out on a PARSTAT 2273 electrochemical wokstation (Princeton Applied Research, USA) in a conventional tree-electrode electrolytic cell with single compartment. A Ti/Pt electrode

(surface area of 2 × 2 cm^2) was used as the counter electrode. A mercurous sulfate electrode (MSE, $Hg/Hg_2SO_4/K_2SO_4$ (saturated), 0.658 V vs. SHE) was used as the reference electrode. All the potentials were quoted with respected to MSE. Before electrochemical tests, the Pb or Pb/AC electrodes were polarized at -1.2 V for 20 min to eliminate the oxides on Pb surface.

Galvanostatic charge-discharge (GCD) tests were carried out on a BTS system (Neware, China). The Pb and Pb/AC electrodes were served as the negative electrodes. The corresponding positive electrode was a commercial pasted PbO_2 electrode (3 mm × 30 mm ×30 mm) with steady potential of 1.075 V in 5 mol L^{-1} H_2SO_4.

EIS was tested at the open circuit potential (OCP) of Pb and Pb/AC electrodes with a voltage amplitude of 10 mV in the frequency range from 100 kHz to 10 mHz. The EIS data was plotted in the forms of Nyquist and Bode (Dependence of phase angle on frequency) plots. The Zsimpwin software was used to simulate the measured data with the designed equivalent circuits. A constant phase element (Q_{dl}) was applied in the equivalent circuit in place of the electric double layer capacitor (C_{dl}), The impedance of a constant phase element can be obtained via Eq. (S1), where n is a dimensionless parameter.[2,3] The values of C_{dl} were calculated via Eq. (S2), where ω'' is the frequency when imaginary impedance is the maximum.[4]

$$Z_{CPE} = \frac{1}{Q(j\omega)^n} \qquad \text{(S1)}$$

$$C = Q(\omega'')^{n-1} \qquad \text{(S2)}$$

Scanning electron microscopy (SEM) images, Energy dispersive spectroscopy (EDS) and

element distribution map were obtained via a SU8020 scanning electron microscope (Hitachi, Japan) coupled with Quantax energy dispersive spectrometer (Bruker, Germany). S-ray diffraction (XRD) patterns were obtained via a Ultima-IV X-ray diffractometer (Rigaku, Japan) with Ni-filtered Cu Ka radiation (λ = 0.15418 nm).

2. Figures and tables in results and discussion section

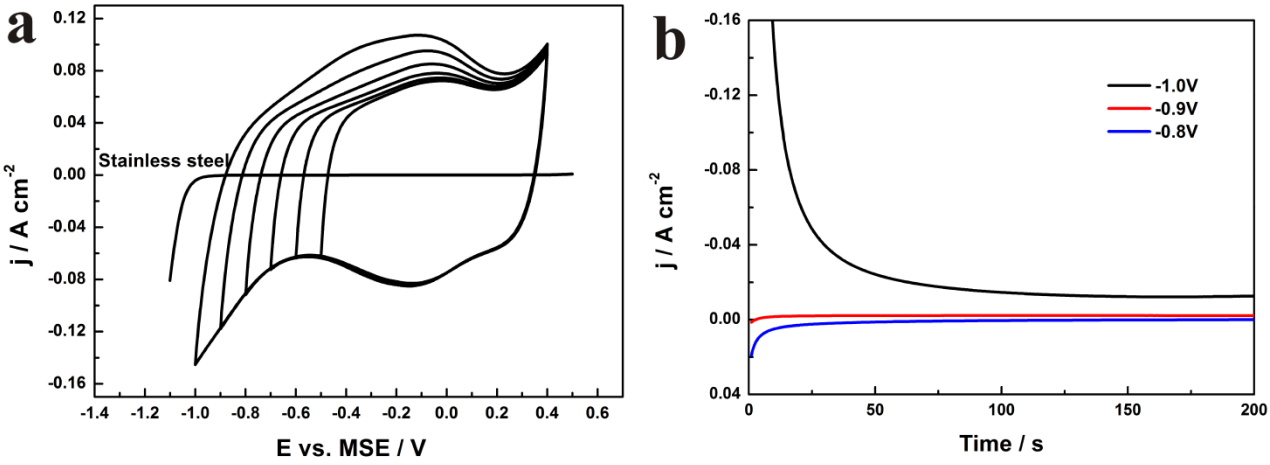

Fig. S2. (a) Cyclic voltammogram of AC, (b) chronoamperometry curves of AC. The AC was tested with stainless steel as current collector to avoid the anodic current of Pb.

The capacitive behavior of AC was tested with stainless steel as current collector by cyclic voltammetry technique (Fig. S2a). Since Pb is passivated at potentials more positive than the OCP of Pb, Pb was not used as current collector in the OCP and cyclic voltammetry tests. The cyclic voltammograms were obtained by fixing the starting potential of cathodic scan (E_{sc}) at 0.4 V, and gradually lowering the starting potential of anodic scan (E_{sa}) with a stepwise of 0.1 V to more negative values. As can be seen from Fig. S3a, AC shows typical capacitive behavior with the E_{sa} of *ca.* -0.6 V, since the voltammogram is a quasi-rectangular shape. When the E_{sa} becomes negative than -0.6 V (the equilibrium potential of water reduction in 5 M H_2SO_4 is -0.617 V vs.

MSE), the shape of voltammogram in cathodic scan showed almost the same, while a noticeable hump due to hydrogen oxidation appeared and gradually increased with lowering E_{sa}. The above results indicate that the H^+ ion is reduced at the inner surface of AC in the cathodic scan and is oxidized in the corresponding anodic scan.[5,6] The chronoamperometry curves (Fig. S2b) show no cathodic (hydrogen evolution) current at -0.9 V and high cathodic current at -1.0 V, indicating the negative confine of the capacitive potential window of AC is -0.9 V. In summary, the AC showed a capacitive behavior from -0.9 V to 0.4 V.

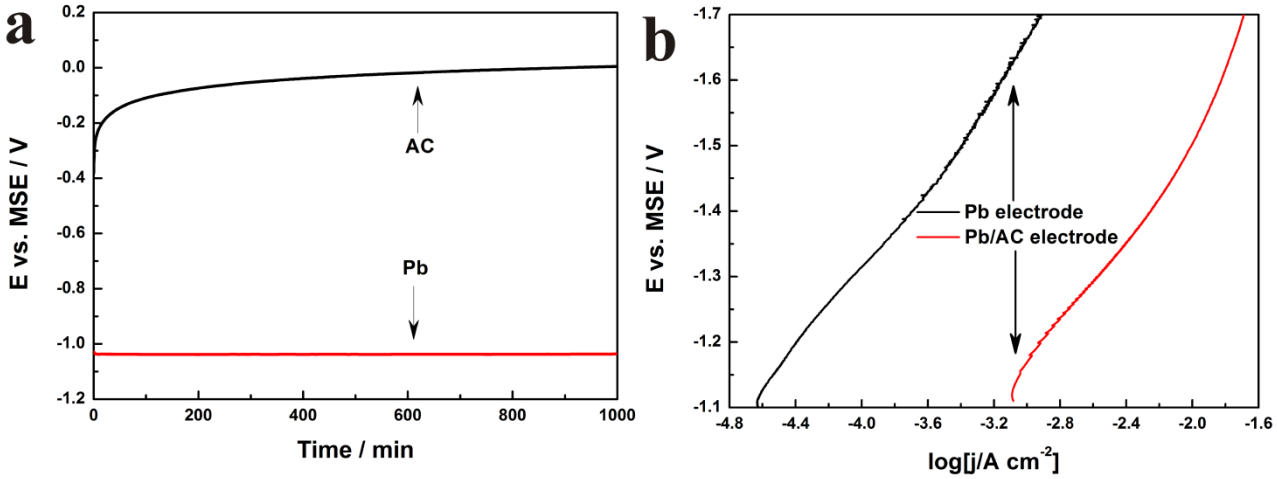

Fig. S3. (a) Open circuit potential transient curves of AC and Pb, (b) Tafel plots of Pb and Pb/AC electrodes.

The OCP transients of AC and Pb electrodes are shown in Fig. S3a. The OCP of AC came to a steady potential at about 0 V,[1] while the Pb electrode had a steady OCP of -1.05 V. The current efficiency of Pb electrode was close to 100%, owing to the high H_2 overpotential of Pb in H_2SO_4 (Fig. S3b). Although, the hydrogen evolution reaction on AC was obvious (Fig. S3b) in the charge potential range of Pb/AC electrode (from -1.1 V to -1.3V), the Pb/AC electrode exhibited high round trip current efficiency of 96-99% in charge-discharge process. The main reason for this

phenomenon was explained in Fig. S8.

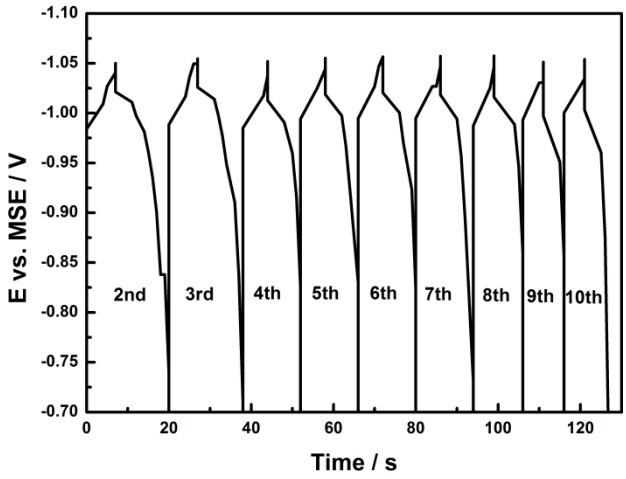

Fig. S4. GCD curves of Pb electrode at current density of 0.5 mA cm^{-2} after 500 GCD cycles at 5 mA cm^{-2}.The Pb electrode showed almost no faradaic capacity in the potential range of -0.7 V to -1.05 V afater 500 GCD cycles at 5 mA cm^{-2}.

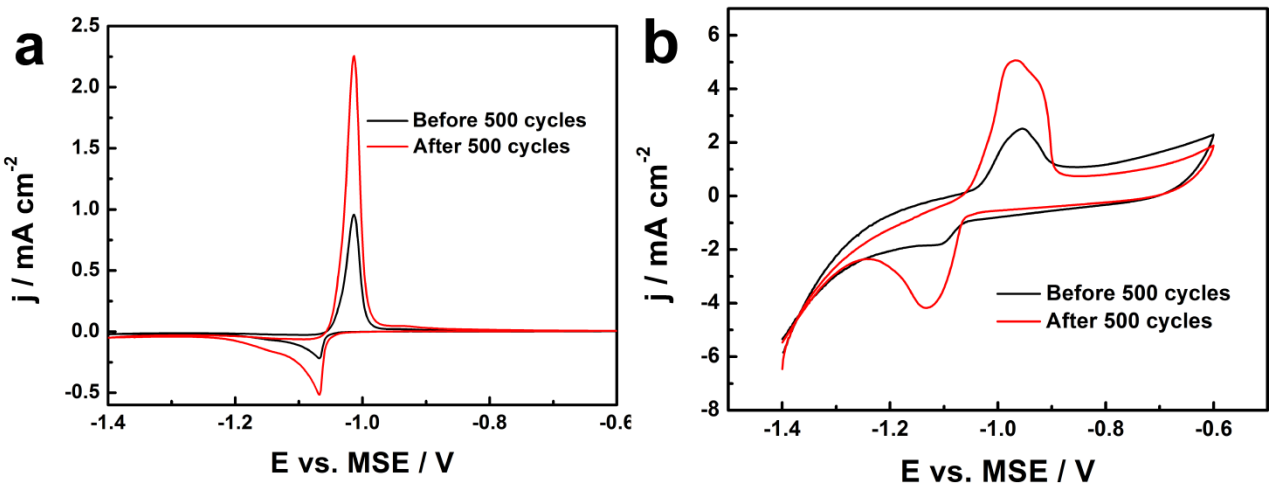

Fig. S5. Cyclic voltammograms of (a) Pb and (b) Pb/AC electrode before and after 500 GCD cycles at 5 mA cm^{-2}.

As can be seen from Fig. S5, the Pb electrode after cycling shows high peak current densities

than the Pb electrode before cycling, which results from the activation of Pb surface[7]. For the Pb/AC electrode before cycling, the cathodic current density is much higher than the Pb electrode before cycling, which is caused by the addition of AC. Since, AC provides large surface area for the electrodeposition of Pb, which enhanced the electrochemical active surface of Pb and the peak current densities. For the Pb/AC electrode after 500 GCD cycles, the peak current is much higher than the Pb/AC electrode before 500 GCD cycles, which is caused by the gradual deposition of Pb on AC surface in the cycling process resulting in the increase of the electrochemical active surface are of Pb.

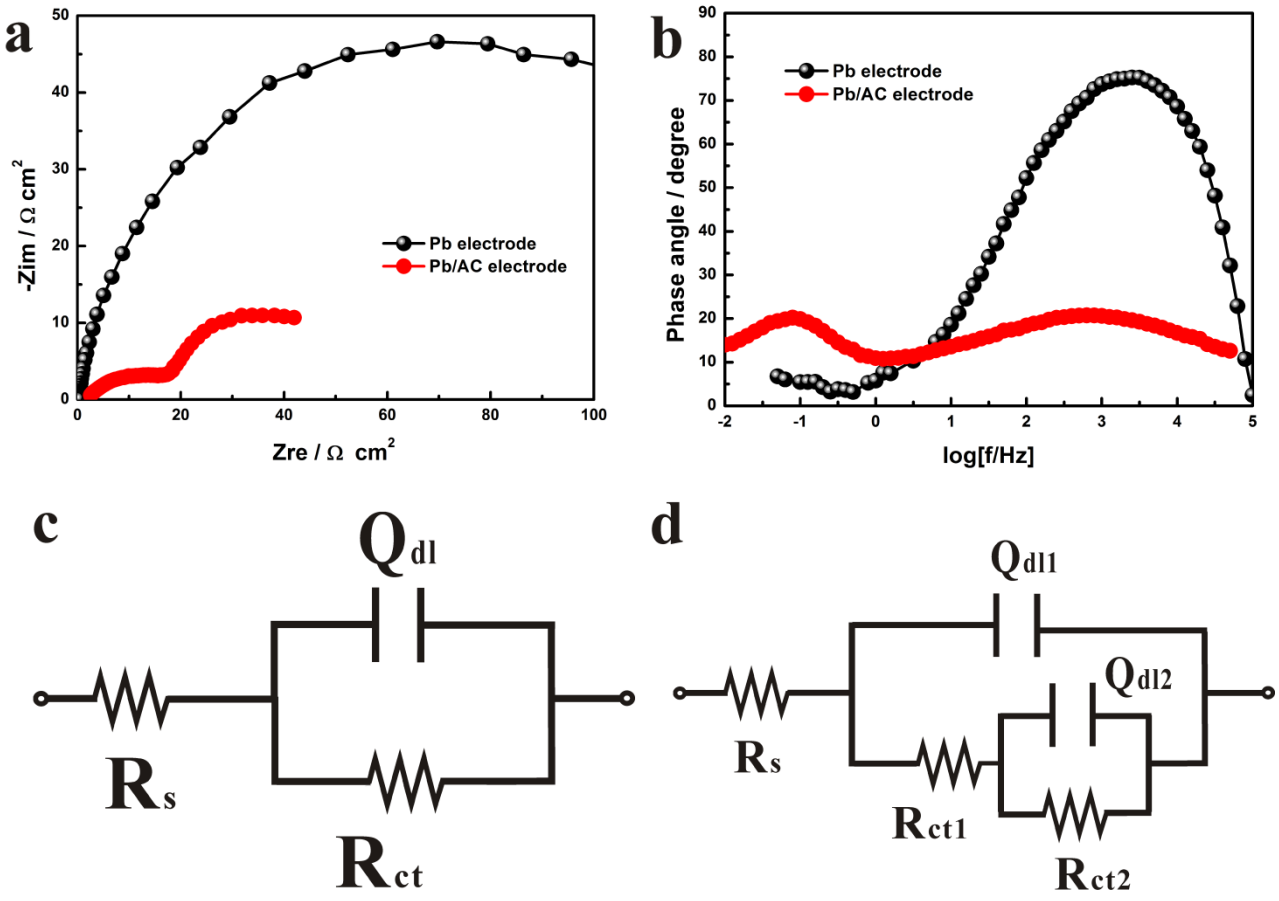

Fig. S6. Electrochemical impedance spectra ((a) Nyquist plot and (b) Bode-phase plot) of Pb

electrode and Pb/AC electrode; Equivalent circuit of (c) Pb electrode and (d) Pb/AC electrode after 500 GCD cycles at 5 mA cm^{-2}.

The electrochemical impedance spectroscopy was used to characterize the charge transfer property of the Pb electrode and the Pb/AC electrode. Fig. S6a and S6b show the Nyquist plot and Bode plot of the two electrodes at OCP. Two different kinds of equivalent circuits were used to characterize the two different electrodes. A Randles circuit (Fig. S6c) was applied to simulate the EIS result of the Pb electrode, representing the charge transfer reaction on the Pb/H_2SO_4 interface. A combined circuit (Fig. S6d) in the form of two RC paralleled circuits was used to characterize the two reactions on the Pb/AC electrode. One reaction represents the charge transfer reaction on Pb/H_2SO_4 interface (R_{ct1}), and the other reaction represents the charge transfer reaction on AC/H_2SO_4 interface (R_{ct2}). The main charge transfer on Pb/H_2SO_4 interface is between Pb and $PbSO_4$, while the main charge transfers on AC/H_2SO_4 interface are both between the redox couples of $PbSO_4$/Pb and H^+/H_2. The elements in each circuit can be distinguished by the subscript of 1 and 2. The simulated results are listed in Table S2 and S3.

Table S2 Simulated values of each element in the equivalent circuit of Pb electrode

R_s	Q_{dl}	n	C_{dl}	R_{ct1}	χ^2
Ω cm^2	Ω^{-1} s^n cm^{-2}	—	F cm^{-2}	Ω cm^2	—
0.3316	5.467×10^{-5}	0.8947	3.132×10^{-5}	132.5	2.173×10^{-3}

Table S3 Simulated values of each element in the equivalent circuit of Pb/AC electrode

R_s	Q_{dl1}	n_1	C_{dl1}	R_{ct1}	Q_{dl2}	n_2	C_{dl2}	R_{ct2}	χ^2
Ω cm^2	Ω^{-1} s^n cm^{-2}	—	F cm^{-2}	Ω cm^2	Ω^{-1} s^n cm^{-2}	—	F cm^{-2}	Ω cm^2	—
1.693	6.949×10^{-3}	0.3961	2.476×10^{-4}	19.49	0.1005	0.7775	0.1368	33.97	1.94×10^{-4}

After 500 GCD cycles, the Pb electrode exhibited a charge transfer resistance of 132.5 Ω cm^2 for the $PbSO_4$/Pb interface. The charge transfer of the Pb/H_2SO_4 interface and the AC/H_2SO_4 interface can be determined by the difference in double layer capacitance (value of C_{dl}). The high capacitance of C_{dl2} (0.1368 F cm^{-2}) represents the double layer capacitance of the AC/H_2SO_4 interface, since the AC has large surface area. The low capacitance of C_{dl1} (0.006949 F cm^{-2}) represents the double layer capacitance of the Pb/H_2SO_4 interface, since Pb has low surface area. The value of R_{ct1} of Pb/AC electrode was 19.49 Ω cm^2 which means that the electrochemical active surface area of Pb was greatly enhanced due to the introduction of AC. The reason is that the lead gradually electrodeposited on the surface of AC forming bulk Pb (Fig. S7), resulting in enhanced electrochemical surface area. The enhanced electrochemical surface area of Pb/$PbSO_4$ interface greatly enhanced the reversibility of the Pb/$PbSO_4$ redox couple.

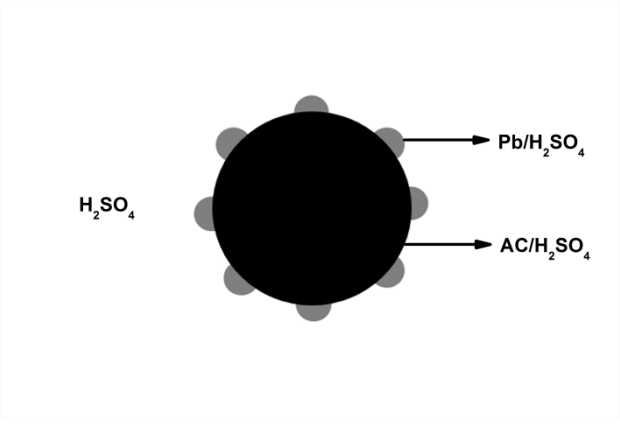

Fig. S7. Schematic diagram of the lead formed on the AC surface and two interfaces

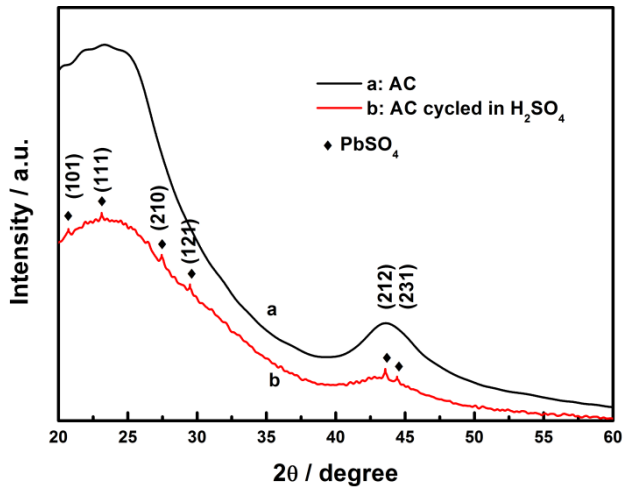

Fig. S8. XRD patterns of AC and AC film tore down from Pb/AC electrode after 500 galvanostatic charge-discharge cycles at 5.0 mA cm^{-2}. The XRD patterns verified the existence of $PbSO_4$.

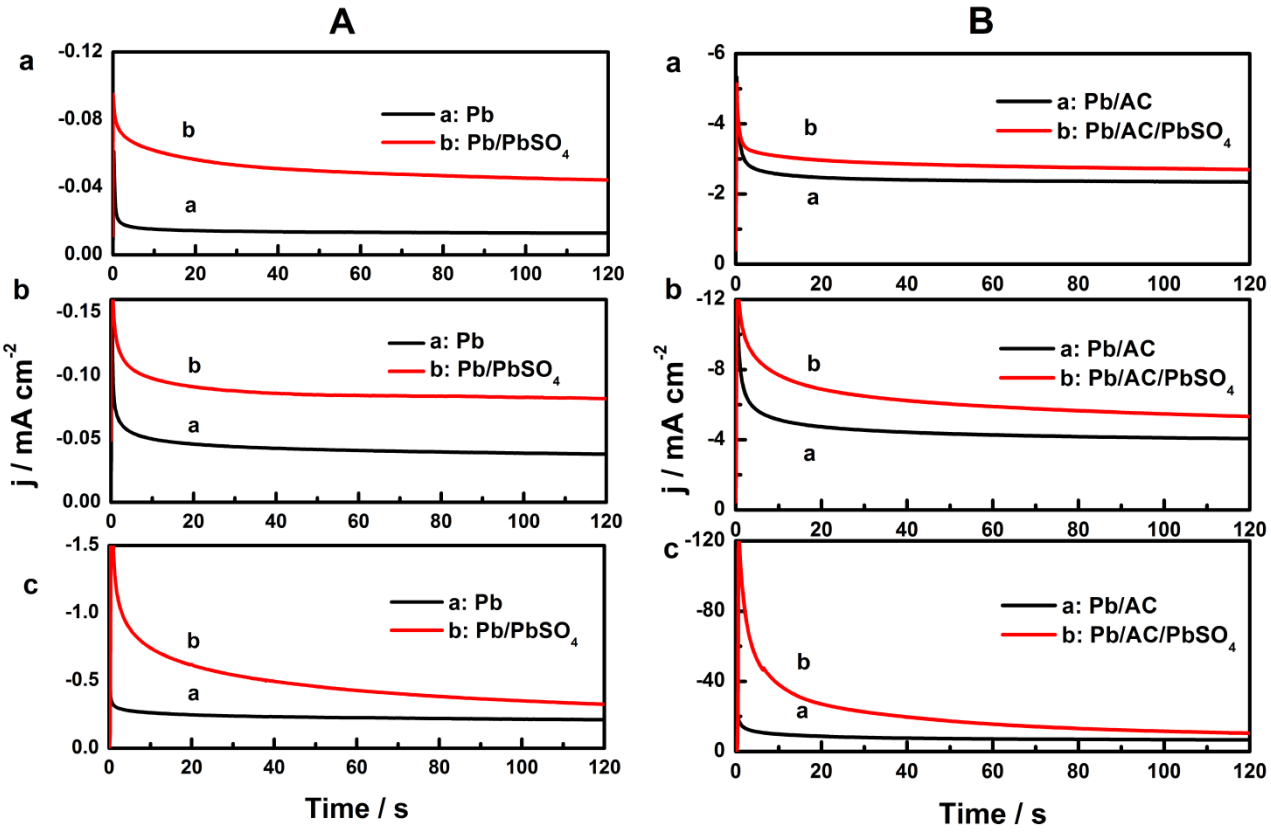

Fig. S9. Chronoamperometry curves of (A) Pb and $Pb/PbSO_4$ electrode, (B) Pb/AC electrode and

Pb/AC/$PbSO_4$ electrode at different hydrogen evolution potentials: (a) -1.1 V, (b) -1.2 V and (c) -1.3 V. The mass loading of $PbSO_4$ on Pb/$PbSO_4$ electrode and Pb/AC/$PbSO_4$ electrode is 100 mg cm^{-2}.

$$AC + H^+ + e^- \rightarrow AC \cdot H \qquad (S3)$$

$$AC \cdot H + H^+ + e^- \rightarrow AC + H_2 \qquad (S4)$$

$$AC \cdot H + AC \cdot H \rightarrow 2AC + H_2 \qquad (S5)$$

Hydrogen evolution behaviors of Pb/AC electrode was studied by the technique of chronoamperometry. As can be seen from Fig. S9a, the hydrogen evolution on a Pb electrode is little. The current response of Pb/$PbSO_4$ electrode decreased gradually due to the diffusion limitation of Pb^{2+}, resulting from the low solubility of $PbSO_4$.[8] While the main reaction on Pb/AC electrode is hydrogen evolution, at the beginning of pulsed potential, Pb/AC has high current response due to the high volume of hydrogen adsorption on the inner surfaces of AC via Volmer reaction (Eq. (S3)).[9] Then the current gradually changed to a steady state (steady hydrogen evolution on AC).

The above results show that if the AC in lead-carbon electrode is charged at high current densities, the HER on AC is unobvious, since there is not enough time for the separation of hydrogen gas from AC surface via Heyrovsky reaction (Eq. (S4)) or via Tafel reaction (Eq. (S5)). At low charge current densities, both elementary steps (Eq. (S3), (S4) and (S5)) have enough time and hydrogen gas separates from the surface of AC, which is the main reason for the low current efficiency at low charge-discharge current densities, even though the Pb electrodeposited on AC

elevates the hydrogen overpotential of AC.[10]

The Pb/AC/$PbSO_4$ electrode has much higher current response compared to the Pb/AC electrode, which is mainly due to the reduction of $PbSO_4$ on AC surface. Since AC has high surface area, the faradaic current related to the reduction of PbSO4 is very high. So in the charge-process of a lead-carbon electrode, the main reactions occurring on AC is the reduction of protons and $PbSO_4$.

References

1 B. Monahov, The beneficial Role of Carbon in the Negative Plate of Advanced Lead-Carbon Batteries, ECS Transactions, 2012, **41**, 45-69.

2 J. B. Jorcin, M. E. Orazem, N. Pébère, B. Tribollet, CPE analysis by local electrochemical impedance spectroscopy, Electrochim. Acta, 2006, **5**1, 1473–1479.

3 E. Barsoukov, J. R. Macdonald, Impedance Spectroscopy: Theory, Experiment, and Applications, Second Edition, Wiley, New Jersey, 2005, p495.

4 W.S. Li, S.Q. Cai, J.L. Luo, Chronopotentiometric responses and capacitance behaviors of passive film formed on iron in borate buffer solution, J. Electrochem. Soc., 2004, **151**, B220.

5 K. Babeł, K. Jurewic, KOH activated lignin based nanostructured carbon exhibiting high hydrogen electrosorption, Carbon, 2008, **46**, 1948-1956.

6 F. Béguin, K. Kierzek, M. Friebe, A. Jankowska, J. Machnikowski, K. Jurewicz, E. Frackowiak, Effect of various porous nanotextures on the reversible electrochemical sorption of hydrogen in activated carbons, Electrochim. Acta, 2006, **51**, 2161-2167.

7 Yoshiaki Yamaguchi, Masashi Shiota, Yasuhide Nakayama, Nobumitsu Hirai, Shigeta Hara, In situ analysis of electrochemical reactions at a lead surface in sulfuric acid solution, 2000, **85**,

22-28.

8 Zen-ichiro Takehara, Dissolution and precipitation reactions of lead sulfate in positive and egative electrodes in lead acid battery, J. Power Sources, 2000, **85**, 29–37.

9 P.S. Fernández, E.B. Castro, S.G. Real, M.E. Martins, Electrochemical behaviour of single walled carbon nanotubes – Hydrogen storage and hydrogen evolution reaction, Int. J. Hydrogen Energy, 2009, **34**, 8115–8126.

10 B. Hong, L. Jiang, H. Xue, F. Liu, M. Jia, J. Li, Y. Liu, Characterization of nano-lead-doped active carbon and its application in lead-acid battery, J. Power Sources, 2014, **270**, 332-341.